American Journal of Sensor Technology, 2017, Vol. 4, No. 1, 10-20
Available online at http://pubs.sciepub.com/ajst/4/1/2

DOI:10.12691/ajst-4-1-2

Electrical and Gas Sensing Behaviour of Polypyrrole/silver Sulphide Nanocomposites

Bharati Yeole, Tanushree Sen, Dharmesh Hansora, Satyendra Mishra*

University Institute of Chemical Technology, North Maharashtra University, Jalgaon, MS
*Corresponding author: profsm@rediffmail.com

Abstract We investigated the room temperature NH_3 sensing performance of polypyrrole/silver sulphide (PPy/Ag_2S) nanocomposites (NCs). Sonochemically synthesized Ag_2S nanoparticles (80-100 nm) were incorporated into the PPy matrix via ultrasound-assisted *in-situ* polymerization. The resulting PPy/Ag_2S NCs were evaluated based on structural, morphological, and electrical properties. Microscopy results revealed a uniform dispersion of Ag_2S nanoparticles in the PPy matrix. We studied the effect of Ag_2S nanoparticle concentration on the electrical properties and gas sensing performance of the PPy/Ag_2S NCs. The current-voltage (I-V) characteristics revealed the semiconducting nature of the PPy/Ag_2S NCs. An improvement in the electrical conductivity was observed for the PPy/Ag_2S NC with 3 wt% Ag_2S nanoparticle content. PPy/Ag_2S NCs were further tested for detection of NH_3 in ambient conditions. The PPy/Ag_2S NCs exhibited excellent sensor response towards 100 ppm NH_3 concentration at room temperature.

Keywords: *silver sulphide, polypyrrole, nanocomposites, ammonia sensing*

Cite This Article: Bharati Yeole, Tanushree Sen, Dharmesh Hansora, and Satyendra Mishra, "Electrical and Gas Sensing Behaviour of Polypyrrole/silver Sulphide Nanocomposites." *American Journal of Sensor Technology*, vol. 4, no. 1 (2017): 10-20. doi: 10.12691/ajst-4-1-2.

1. Introduction

Nanosensors are characterized by remarkable physical properties owing to the significantly high surface area to volume ratio that is unique to nanoscale materials. They provide advantageous performance advantages such as sensitivity that is orders of magnitude higher than that of conventional sensors, and fast response and response times. Nanosensors can perform as autonomous systems or can be build into integrated systems or networks. Moreover, the extremely small size of the sensing element allows for the building of portable devices. The detection of chemical and biological species is central to many areas of environment health, healthcare, and occupational safety. Many materials have been used as nanosenors for a variety range of applications [1,2,3]. Among these materials, intrinsically conducting polymers (ICP) have demonstrated immense potential in the field of sensors, energy storage and nanoelectronics, owing to their attractive mechanical, electrical, physical, and structural properties. The advantage of ICPs, as nanosensors, lies in its usability in ambient conditions and room temperature. Further inclusion of a secondary component such as nanoparticles (NP) in the ICP matrix is another factor that influences the electrical properties of ICPs. This has led to a surge in research concerning the development of polymer nanocomposites (PNCs) for nanosensor applications. Metals and metallic compounds offer a synergistic effect when combined with ICPs [4,5,6,7]. Metal oxides [4,8-14] and metal sulphides [10,11] have been widely used for the detection of various analytes [5,15,16]. Roy et al. [17,18,19] have synthesized a range of polyaniline (PANI) composites with metal oxide and calcium titanate, which exhibit remarkable electronic and electrical properties. Parveen et al. [20] have reported a significant response of 90% towards liquefied petroleum gas (LPG) using PANI/TiO_2 nanocomposites. In another study, they reported a highly sensitive PANI/$CaTiO_3$ nanocomposite based humidity sensor operating in the temperature range of 40-200°C [21]. Roy et al. [22] have reported a highly selective LPG sensor based on PANI/CdO nanocomposites. However, operations at high temperatures affect the structure and performance of the sensor. Hence, sensors based on ICPs, that are operable at room temperature, can overcome this issue [4,5,6,7,8,23,24]. When combined with NPs, the ICP based sensors show an enhancement in sensitivity and selectivity. The most relevant feature, amongst the properties of ICP that are affected by analyte adsorption, is the electrical property [25,26,27,28,29]. The parameters that influence the sensor performance are polymerization method, type of oxidants, type of dopants and level of doping, and reaction temperature [10,11,12,30].

Polypyrrole (PPy) is one of the most researched ICP owing to its high chemical and environmental stability as well as electrical conductivity [9,10,11,12,28,29,30]. Ease of synthesis, low cost and easy availability of the pyrrole monomer, and the possibility of bulk production add to its popularity amongst the ICPs. Doped PPy generally behaves like a p-type semiconductor and has been used for the detection of a variety of analytes [31]. The properties of polymer–inorganic NPs hybrid NCs depend on the properties of its constituents, the volume fraction of

components, the shape and arrangement of inclusions, and the interfacial interaction between the matrix and the NPs [32]. In combination with NPs, PPy based NCs have already shown an improvement in electrical conductivity, and hence, gas sensing response [6,32,33,34]. Silver sulphide (Ag_2S) is an inorganic semiconductor material that has been used for the preparation of PNCs for application in electrochemical devices and solar cells [14]. Chih and Yang [35] have reported the detection of dopamine by Ag_2S modified carbon nanotube (CNT) based NCs. PPy nanotubes filled with Ag/AgCl have also been studied [36]. Similarly, silver NPs decorated PPy NCs were studied for electrocatalysis and antibacterial properties [37].

Ammonia (NH_3) detection at low concentrations is crucial in many technological fields, such as food technology, chemical engineering, medical diagnosis, environmental protection, monitoring of car interiors, and industrial processes. The threshold limit of NH_3 concentration in air is 24 ppm; the presence of a high concentration of NH_3 in the atmosphere is potentially toxic and harmful, causing irritation of the skin, eyes, and respiratory system. Several researchers have reported that NH_3 can be detected using various polymers and metal oxides and their composites with high sensitivity at both lower and higher measuring temperatures [10,11,12,24]. Presently, researchers are focusing on the development of low cost, small-sized, portable devices that can be used in real-time monitoring. However, high operating temperatures pose a hindrance in the detection of flammable gases, and can cause instability in the sensing devices; these factors can significantly lower the sensor's reusability, thus resulting in high maintenance cost [6,10,11,12].

Limited literature is available on the detection of NH_3 by PPy or its nanocomposites [38-43]. We have previously reported the room temperature detection of various analytes by PPy nanocomposites and elucidated the underlying sensing mechanisms for the same [10,44]. In the present work, Ag_2S NPs (80-100 nm) were sonochemically synthesized and incorporated in variable amounts (1-3 wt%) into the PPy matrix via *in-situ* polymerization under ultrasound at room temperature. The PPy/Ag_2S NCs were characterized using various spectroscopic techniques viz. Fourier transform infrared (FTIR) spectroscopy, ultraviolet-visible (UV-vis) spectroscopy, and X-ray diffraction (XRD). The surface morphology and elemental analysis of PPy, Ag_2S NPs, and PPy/Ag_2S NCs were ascertained by field emission scanning electron microscopy (FE-SEM) and energy dispersive X-ray (EDX) spectroscopy, respectively. The current-voltage (I-V) characteristics of these pellets were measured by four-point probe method. We investigated the influence of the varying contents of Ag_2S NPs on the electrical properties and the NH_3 sensing performance of the PPy/Ag_2S NCs at room temperature. We evaluated the sensing performance of PPy/Ag_2S NCs towards different concentrations (100 to 500 ppm) of NH_3 and proposed a mechanism for the said observation.

2. Experimental

2.1. Materials

Analytical grade pyrrole, anhydrous ferric chloride ($FeCl_3$), and HCl were purchased from Merck (Mumbai, India). Sodium lauryl sulphate (SLS) and silver nitrate ($AgNO_3$) were procured from S.D. Fine Chem. Ltd. Mumbai, while sodium sulphide (Na_2S) was purchased from Himedia Laboratories Pvt. Ltd. (Mumbai, India). Acetone and methanol used for washing purposes were procured from S.D. Fine Chem. Ltd. (Mumbai, India). Ultra-pure water from Smart 2 Pure system (Thermo Electron LED GmbH, Germany) was used for preparing solutions, in the synthesis of NPs and NCs, and for cleaning and washing purposes. NH_3 gas was purchased from Master Specialty Gases Pvt. Ltd. (Mumbai, India). Microscope glass slides (Polar India Corporation, Mumbai) were used for the deposition of PPy/Ag_2S NCs films.

2.2. Ultrasound-assisted Synthesis of Ag_2S Nanoparticles

Ag_2S NPs were sonochemically synthesized using an ultrasound probe (BO3 Ultrasonic Processor UP1200, Cromtech, India). An excess of 0.5 M Na_2S solution was dropwise added to an aqueous solution of 0.005 M $AgNO_3$ under ultrasound environment. The conversion of $AgNO_3$ to Ag_2S occurs as follows.

$$\mathbf{2AgNO_3 + Na_2S \rightarrow Ag_2S + 2NaNO_3}.$$

The reaction mixture was stirred at room temperature (~ 30±2°C). Black precipitate of Ag_2S was obtained after 12 h, which was centrifuged at 8000 rpm, washed with acetone and water, and then dried in a vacuum oven at 60°C for 30 min.

2.3. Synthesis of PPy and PPy/Ag_2S Based Nanocomposites

PPy and their PPy/Ag_2S NCs were synthesized by chemical oxidative polymerization. An aqueous solution of $FeCl_3$ (oxidant) was added dropwise to an aqueous solution of pyrrole (monomer) under continuous stirring at 30±1°C. The mole ratio of pyrrole to $FeCl_3$ was kept as 1:2.33 [10]. Two treated glass slides (cleaned by immersion in 0.1 M aqueous HCl solution, and successive sonication in water and methanol) were placed in the beaker containing pyrrole solution. PPy/Ag_2S NCs were prepared by ultrasound-assisted *in-situ* polymerization. First, predetermined amount of Ag_2S NPs were ultrasonically dispersed in the pyrrole solution. Next, the oxidant was added to the monomer solution to facilitate polymerization. The reaction conditions for NC preparation were the same as mentioned above for PPy formation. After the complete addition of $FeCl_3$, the reaction was stirred for 2 h and then allowed to stand overnight. The glass slides, with *in situ* deposited PPy and PPy/Ag_2S NCs films, were taken out, washed with water and ethanol, and then dried under vacuum for 2 h. The films formed in $FeCl_3$ solution were observed to be blue-black in color, which confirmed that the films were fully oxidized [10,12,29]. The blue-black PPy and PPy/Ag_2S NCs precipitates were repeatedly washed with water and acetone, and then dried at in a vacuum oven at 60 ^oC for 8 h. Similarly, PPy/Ag_2S NCs were prepared by adding varying amount of Ag_2S (1, 2, and 3 wt%), which are henceforth referred to as A1, A2, and A3, respectively.

2.4. Preparation of Pellets

PPy and PPy/Ag_2S NCs were formed into pellets by using a Hydraulic Press Machine (Kimaya Engineering, Mumbai). Approximately 2 mg of dried powder (PPy and PPy/Ag_2S NCs) sample was placed between two die plates and then pressurized by the hydraulic press to obtain pellets having a diameter of 10 mm and a thickness of 2 mm. These pellets were used for electrical measurements and NH_3 gas sensing.

2.5. Characterization

2.5.1. Fourier Transforms Infrared (FTIR) Spectroscopy

Pristine PPy and PPy/Ag_2S NCs were prepared into pellets by mixing with potassium bromide (KBr) and their FTIR spectra were recorded on a Shimadzu FTIR-8400 spectrophotometer (Tokyo, Japan) within the wavenumber range of 400–4000 cm^{-1}.

2.5.2. UV-visible Spectroscopy

UV–vis absorption spectra of pristine PPy and PPy/Ag_2S NCs dispersed in DMF (0.1 mg sample/20 mL of DMF) were recorded on a Hitachi U-2900 spectrophotometer (Tokyo, Japan) in the range of 200–800 nm.

2.5.3. X-ray Diffraction (XRD)

XRD analysis of pristine PPy and PPy/Ag_2S NCs (A1, A2, and A3) was conducted on a Advance X-ray diffractometer (Brukers D8, Germany) with $CuK_{\alpha 1}$ radiation (λ = 1.5404 Å) in the 2θ range of 10° - 60°.

2.5.4. Field Emission Scanning Electron Microscopy (FE-SEM) and Energy Dispersive X-ray (EDX) Spectroscopy

The surface morphology of PPy and PPy/Ag_2S NC films was assessed using a field emission scanning electron microscope (Hitachi S-4800, Tokyo, Japan). The samples were mounted on a specimen stub and carbon-coated before viewing under the microscope. The elemental compositions of Ag_2S NPs and the PPy/Ag_2S NCs were studied using EDX spectroscopy.

2.5.5. Current-voltage (I–V) Characteristics

The electrical conductivity of PPy and PPy/Ag_2S NC pellets was measured by four-point probe conductivity meter connected to a constant current source (CCS-01) and a micro voltmeter (DMV-001, SES Instruments, Scientific Equipments, Roorkee, India). The four equally spaced probes were made of tungsten metal and were mounted on a Teflon bush sheet, which ensured a good electrical insulation between the probes. The probes were individually spring loaded to minimize the sample damage during measurement. A Teflon spacer near the tips was also provided to keep the probes at equal distance. The advantage of the four-point probe over the conventional two-probe method is that it prevents error due to contact resistance. The whole–arrangement was mounted on a suitable stand and leads were provided for current and voltage measurement. The current source was a circuit regulated current generator that provided a constant current to the outer probes. It has the ability to measure 0-200 mA up to 10 V. The electrical conductivity, which is reciprocal of the electrical resistivity, was calculated from the current-voltage (I-V) graph using equation (1), where V is the voltage in volts, I is the current, and s is the distance between the probes (2 mm).

$$\text{Electrical conductivity} = \frac{1}{\left(\frac{V}{I}\right)2\pi s}. \quad (1)$$

2.5.6. Measurement of NH_3 gas Sensitivity at Room Temperature

Pellets of PPy and PPy/Ag_2S NCs (A1, A2, and A3) were individually loaded into a sensing chamber (Vijay Scientifics, Aurangabad, India) and two conducting probes were connected to the pellets through silver contacts (Figure 1). Glass slides were used to support the pellets. The resistances of the PPy/Ag_2S NC sensors were obtained with the help of a programmable 4.5 digital multimeter (SM 5015, Scientific MES-Technik Private Limited, Indore, India) connected to a computer through RS232C interface. First, the electrical measurements of the samples were taken in air. Thereafter, NH_3 gas was injected into the chamber at different concentrations (100, 250 and 500 ppm) and the change in the I-V characteristics was recorded. The electrical measurements of the pellets of PPy and PPy/Ag_2S NCs were recorded in the bias range of 0.15 to −0.15 V and their electrical conductivities were deduced from the I–V graphs using equation (1). The response factor of each of the PPy and PPy/Ag_2S NC pellets was recorded first in air and then in the presence of different concentrations of NH_3 gas (100, 250, and 500 ppm). All electrical measurements were taken at room temperature (30±2°C). The normalized response of the sensors in the presence and absence of NH_3 gas was calculated using equation (2), where I_a is the current of the sample in the presence of air and I_g is the current of the sample in the presence of gas.

$$\text{Gas response factor} = \left(\frac{I_a - I_g}{I_a}\right). \quad (2)$$

3. Results and Discussion

3.1. Formation of PPy and PPy/Ag_2S NCs

PPy and PPy/Ag_2S NCs were prepared via oxidative polymerization at room temperature. The properties of the resulting polymer are affected by the mole ratio of the monomer to the oxidant, which has been already optimized as 1:2.33 [9,10,29]. During the oxidative polymerization of pyrrole, the electro-neutrality of the polymer chain is maintained by the anions that are incorporated from the reaction mixture. These counter-anions are usually generated from the chemical oxidants or the reduced products of the oxidants, for example, Cl^- ion from the oxidant $FeCl_3$ [9,10,15,29]. The formation of PPy via oxidative polymerization of pyrrole using $FeCl_3$ as the oxidant has been shown in Scheme 1. Initially, pyrrole is oxidized by Fe^{3+} ion to give pyrrole radical cation.

This is followed by the dimerization of the radical cations with the expulsion of two protons. Subsequently, chain propagation occurs via the addition of a new radical cation.

In the preparation of PPy/Ag_2S NCs, as depicted in Figure 2, the newly formed oligomeric units adhered to the NP surface which served as the nucleation sites. As polymerization proceeded, these NPs were embedded into the PPy matrix. The ultrasound-assisted *in-situ* polymerization method for the preparation PPy/Ag_2S NCs, therefore, has dual advantages: (i) it prevents the aggregation of NPs due to the presence of ultrasound environment and (ii) the NPs are uniformly embedded into the PPy matrix. Therefore, the ultrasound plays a crucial role in the formation of NCs with respect to their uniform dispersion in the monomer solution, which is an important criterion for the optimal performance of NCs.

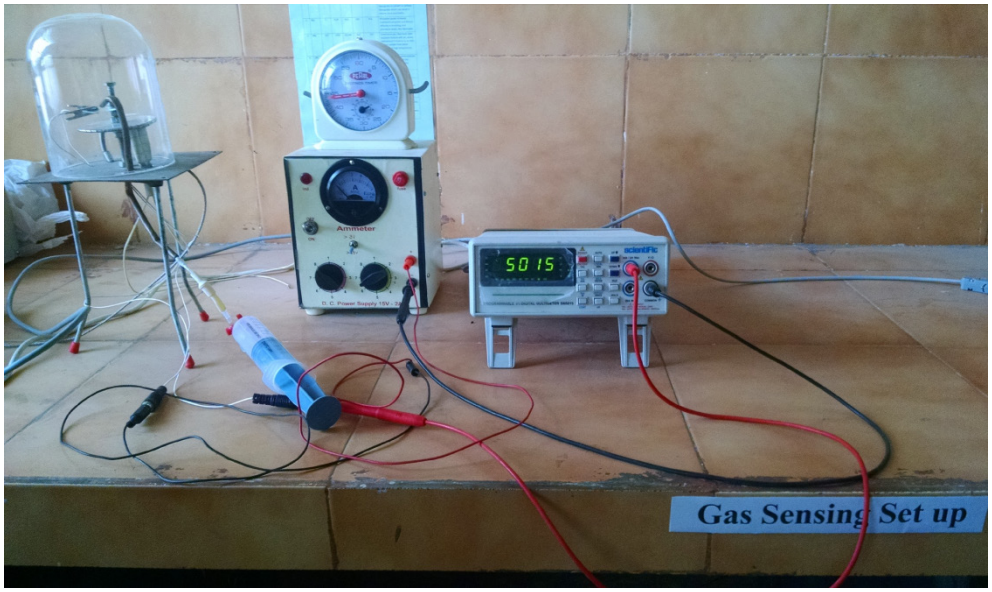

Figure 1. Gas sensing apparatus

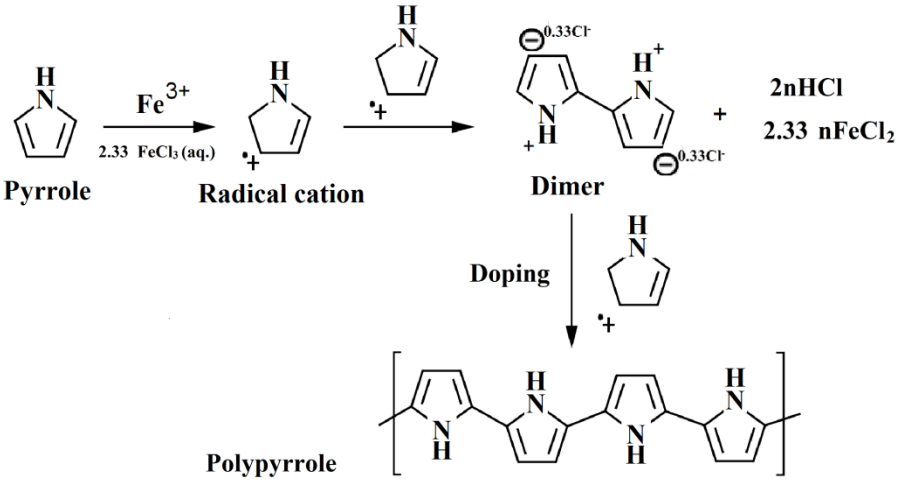

Scheme 1. Oxidative polymerization of pyrrole

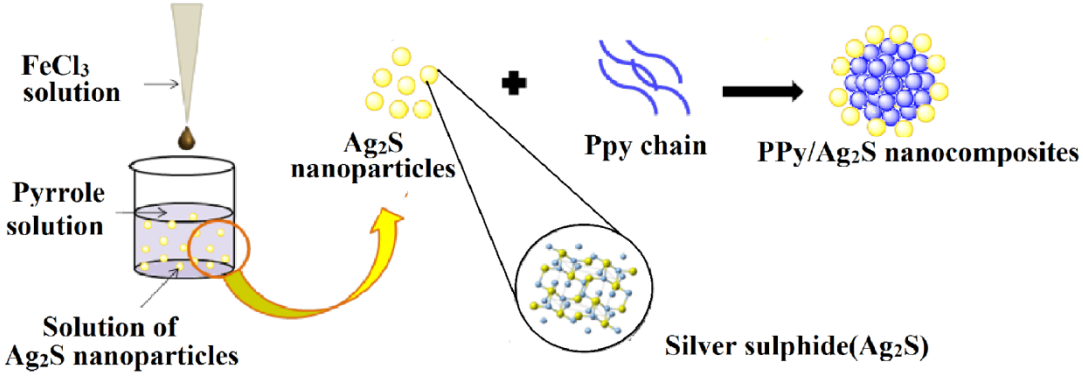

Figure 2. Pictorial representation of formation of PPy/Ag_2S NCs

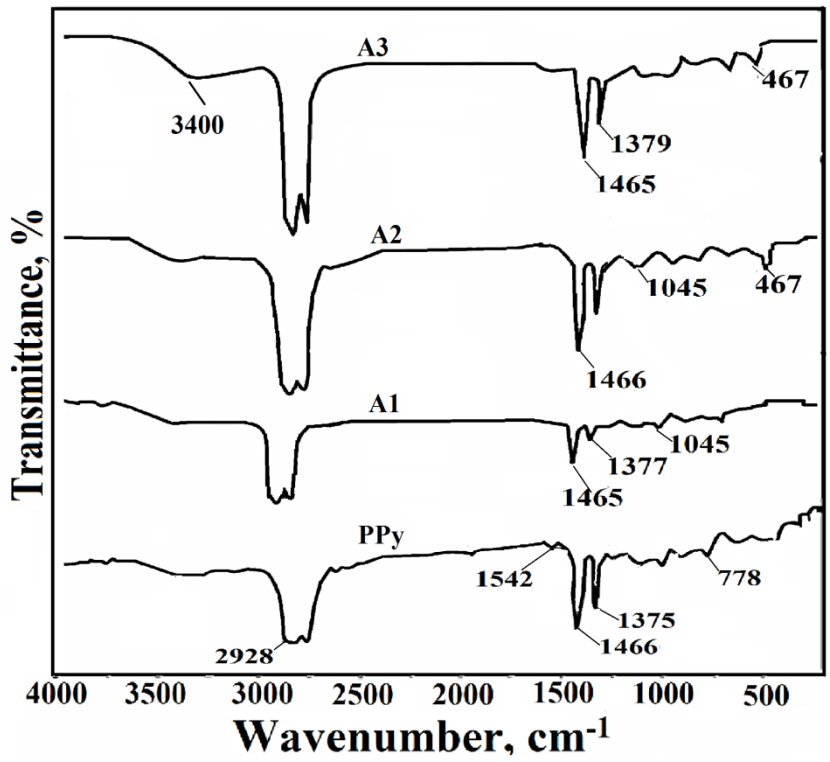

Figure 3. FTIR spectra of PPy and various PPy/Ag_2S NCs

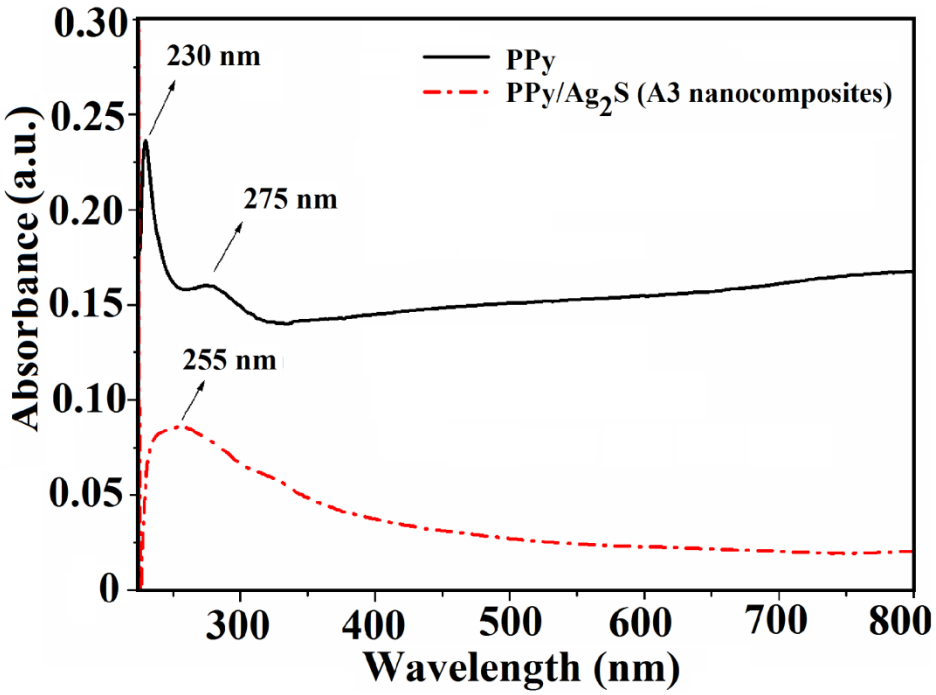

Figure 4. UV absorption of PPy, PPy/Ag_2S (3 wt%) NCs (A3)

3.2. FTIR Studies

The characteristic functional groups in PPy and PPy/Ag_2S NCs can be seen from their FTIR spectra in Figure 3. The IR spectra for pyrrole displayed intensive narrow bands for in-plane deformation vibrations of δ_{pl} (C-H) at 1015, 1045, and 1075 cm^{-1} [32]. After the addition of $FeCl_3$ to the pyrrole solution, new bands at 1100, 1125, and 1150 cm^{-1} appeared against the background of the pyrrole bands. The intensity of these new bands increased with time, while that of the pyrrole vibrations simultaneously decreased. The mutual arrangement of these bands suggested that they refer to the deformation vibrations of the pyrrole ring in a PPy complex [9]. The peak around 1045 cm^{-1} can be assigned to N-H in-plane deformation [11], while the peak at 778 cm^{-1} is due to C-N out-of-plane deformation in PPy [6]. The other peak positions can be assigned to the characteristic vibration modes of PPy molecules: C-O bending at 1125 cm^{-1} and C=C ring stretching at 1640 cm^{-1} [6,11]. The peak around 1375-1379 cm^{-1} is related to the vibration of C-H stretching in the PPy ring. The fundamental vibrations of pyrrole ring,

observed at 1542 and 1466 cm^{-1}, can be assigned to the C=C and C-C ring stretching modes, respectively [6,29]. The broad peak at about 3400 cm^{-1} arises due to N-H stretching vibrations [6,29]. These results indicated that the extent of oxidation of PPy increased by increasing the molar ratio of the oxidant and the monomer. The wavenumber shift (1551-1563 cm^{-1}) of the N-H band confirms the formation of hydrogen bonds on the PPy backbone as well as also for ring stretching in pyrrole ring [25,32]. The peak around 1045 cm^{-1} can be assigned to C-H in-plane deformation while the peak at 778 cm^{-1} is due to C-H out of plane deformation in PPy. The peak at 2928 cm^{-1} is possibly associated with CH_3 stretching vibrations in N-methyl pyrrole unit. A peak near around 467 cm^{-1} can be observed in the spectra of the all PPy/Ag_2S NCs, which is associated with the Ag_2S NPs present in the PPy/Ag_2S based NCs. The result indicates strong interaction between PPy and the Ag_2S NPs.

3.3. UV-visible Spectra

Figure 4 presents the UV–vis spectra of PPy and PPy/Ag_2S (3 wt%) NCs (A3). Pristine PPy shows a strong absorption band at ~ 230 nm in the UV region, which is due to π-π* transition [10]. A slight shoulder is also observed at ~ 275 nm due to the π electron system in PPy. The progressive increase of the absorption bands, which is associated with the character of the chemical bond between the pyrrole rings in PPy and the chlorine anions from $FeCl_3$, is indicative of PPy formation through polymerization [9].

The PPy films exhibited absorption peaks at 442 nm [6,32]. An absorption peak of PPy/Ag_2S NC (A3) was observed at ~ 255 nm. The shift in peaks in the spectrum of the nanocomposite is indicative of interactions between the Ag_2S nanoparticles and the PPy chains [6]. The calculated bandgap, E_g, corresponding to the π-π* transitions in PPy and PPy/Ag_2S NC (A3) were reported to be 0.22 and 0.20 eV, respectively. Hence, a nearly similar electrical conductivity can be expected of PPy and its nanocomposites. The shift in the absorption peaks in the spectrum of the PPy/Ag_2S NC strongly suggests an interaction between the Ag_2S NPs and the PPy chains.

3.4. Phase Identification

Figure 5(a-b) shows the XRD spectra of PPy, Ag_2S NPs, and PPy/Ag_2S NCs. A broad diffraction peak at 24° is associated with the (1 1 2) plane of PPy and shows its amorphous nature [6,10,32]. In general, doping leads to shifting of peaks toward a higher angle due to a decrease in the interplaner spacing. The addition of dopants brings the polymer chains closer as a result of a greater overlap of π-bonds, which consequently increases the electrical conductivity.

For Ag_2S NPs, the observed peaks have the d-values 3.08, 2.6, 2.58, 2.45, and 2.21 nm corresponding to the (1 1 1), (1 2 0), (0 2 2), (1 1 2), and (0 3 1) planes, respectively. The crystal size of Ag_2S NPs was reported to be 61.2 nm and the crystallinity was ~ 70.6%. The PPy/Ag_2S (1, 2, and 3 wt%) NCs (A1, A2, and A3) showed additional diffraction peaks (Figure 5(b)) near 27°, 31°, and 46° associated with (0 1 2), (1 2 0) and (2 2 1) planes of Ag_2S NPs, respectively. The crystallinity of PPy/Ag_2S nanocomposites (A1, A2 and A3) were recorded as 49.6, 58, and 70 %, respectively, indicating the influence of Ag_2S nanoparticles on the ordering of the PPy chains resulting in an increased crystallinity with increasing Ag_2S content.

3.5. Surface Morphology

Spherical Ag_2S NPs with a diameter of ~53 nm (± 5 nm) can be observed in the FE-SEM micrographs, as shown in Figure 6(a). Globular and porous PPy were formed with a diameter of ~350 nm, as can be clearly seen in (Figure 6(b)). A micrograph in Figure 6(c) shows the uniform distribution of Ag_2S NPs in the the PPy/Ag_2S (3 wt%) NCs (A3). It is evident from the FE-SEM result (Figure 6(a) and Figure 6(c)) that the ultrasound induced cavitation produced nanostructures without any aggregation and also aided in the uniform dispersion of NPs in the polymer matrix [4,10]. With an increase in the content of Ag_2S NPs in the PPy matrix, the morphology changed to overgrown clusters and porous interconnected nanospheres [32]. The EDX spectrum of Ag_2S NPs in Figure 7(a) shows Ag and S, and peaks with the composition as Ag = 73.37 wt% and S = 23.69 wt% confirming the formation of Ag_2S. The EDX spectrum of PPy/Ag_2S NC (Figure 7(b)) exhibited peaks of Ag and S along with C and N; the composition of the PPy/Ag_2S NC was C = 54.5 wt%, Ag = 25.63 wt%, and S = 14 wt%. The EDX results confirmed the presence of Ag_2S NPs in the PPy matrix in PPy/Ag_2S NCs.

3.6. Current-voltage (I–V) Characteristic

I-V characteristics of PPy and the PPy/Ag_2S NCs are presented in Figure 8. It can be observed that pristine PPy has an ohmic behavior and hence a semiconducting nature [6,29]. The electrical conductivity of pristine PPy was calculated as 1.9×10^{-3} $S \cdot cm^{-1}$. The conductivity values of the PPy/Ag_2S (1, 2, and 3 wt%) NCs (A1, A2 and A3) was calculated as 3.8×10^{-4}, 5×10^{-4}, and 3.9×10^{-3} $S \cdot cm^{-1}$, respectively. It should be noted that an increase in the Ag_2S NP content of up to 2 wt% resulted in a drop in the electrical conductivity, whereas at 3 wt% Ag_2S NP content the conductivity of the NC (A3) was more than that of PPy. A possible explanation for this is the varying dispersion of Ag_2S NPs in the A3 nanocomposite. The initial drop in conductivity can be attributed to localization of charge in the p-type PPy by the n-type Ag_2S nanoparticle. However, with an increase in the Ag_2S NP content, the percolation threshold in the PPy/Ag_2S NC is reached; this created an efficient electric channel in the NC that manifested as a sudden increase in the electrical conductivity of the A3 nanocomposites.

3.7. Gas sensitivity at Room Temperature

NH_3 is a colourless, flammable gas and forms explosive mixture with air at ~ 16 - 25%. It is highly toxic and has a permissible exposure limit of 25 ppm. Exposure to over 500 ppm concentration of NH_3 is lethal for humans as well as land and aquatic animals. Although its odor is detectable below 50 ppm, repeated exposure lowers the sensitivity to its odor. NH_3 is commonly present in fertilizers, household cleaners, and in compressors of air

conditioners. NH_3 is also an important component in the industrial production of synthetic polymers and explosives. It is because of these reasons that detection of NH_3 gas at room temperature is necessary.

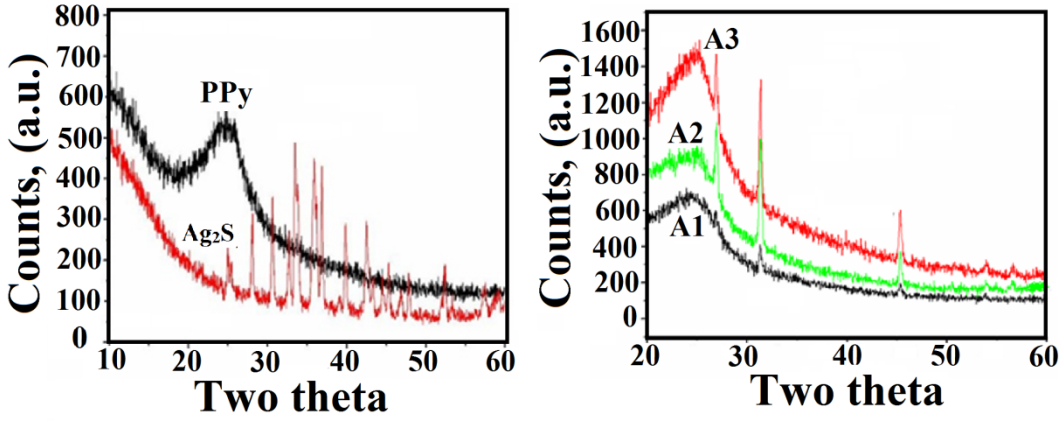

Figure 5. XRD of (a) Pure PPy, (b) Ag_2S NPs, and (c) various PPy/Ag_2S NCs

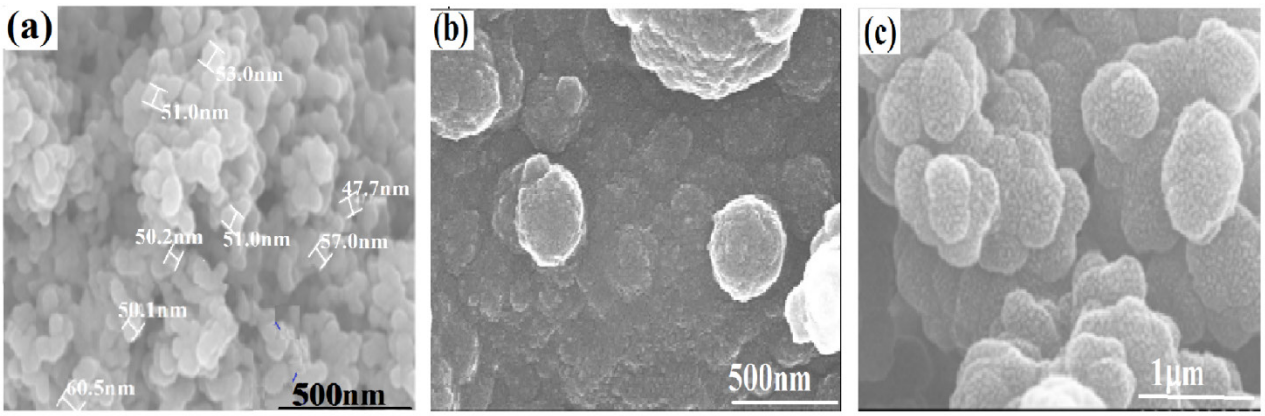

Figure 6. SEM micrographs of (a) Ag_2S NPs, (b) PPy, and (c) PPy/Ag_2S NCs

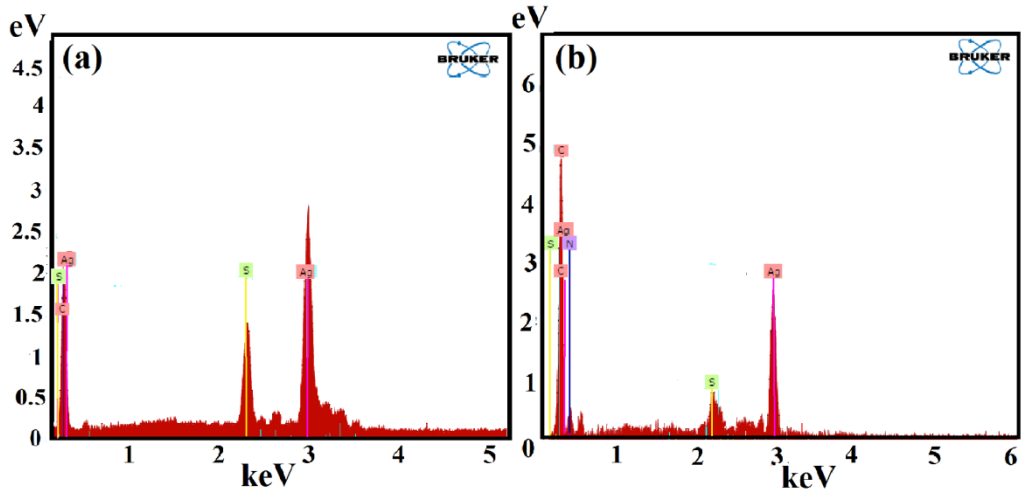

Element	Atomic No.	Wt.	Normal Composition Weight %	Atomic Composition Atom %
C	6	8.67	2.94	3.34
S	16	69.87	23.69	71.88
Ag	47	216.37	73.37	24.78
Total :		294.91	100	100

Element	Atomic No.	Wt.	Normal Composition Weight %	Atomic Composition Atom %
C	6	10.03	54.51	69.76
N	7	1.07	5.84	1.02
S	16	2.58	14.00	1.09
Ag	47	4.72	25.63	28.13
Total :		18.40	100	100

Figure 7. EDX pattern of (a) Ag_2S NPs and (b) PPy/Ag_2S NCs

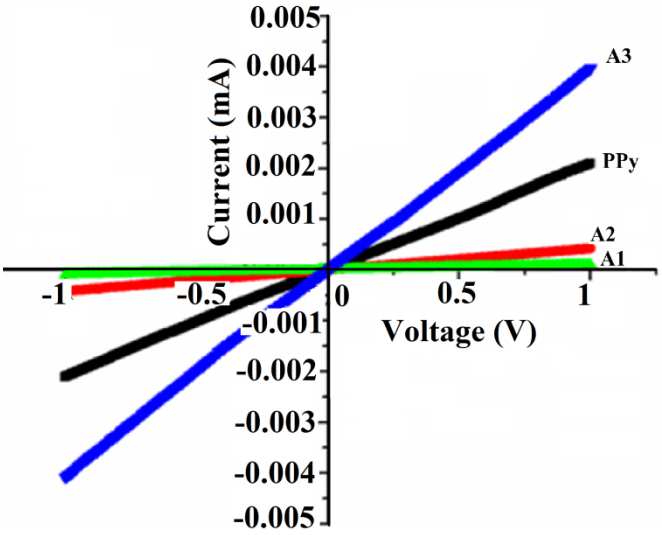

Figure 8. Electrical (I-V) characteristics of PPy and PPy/Ag_2S NCs

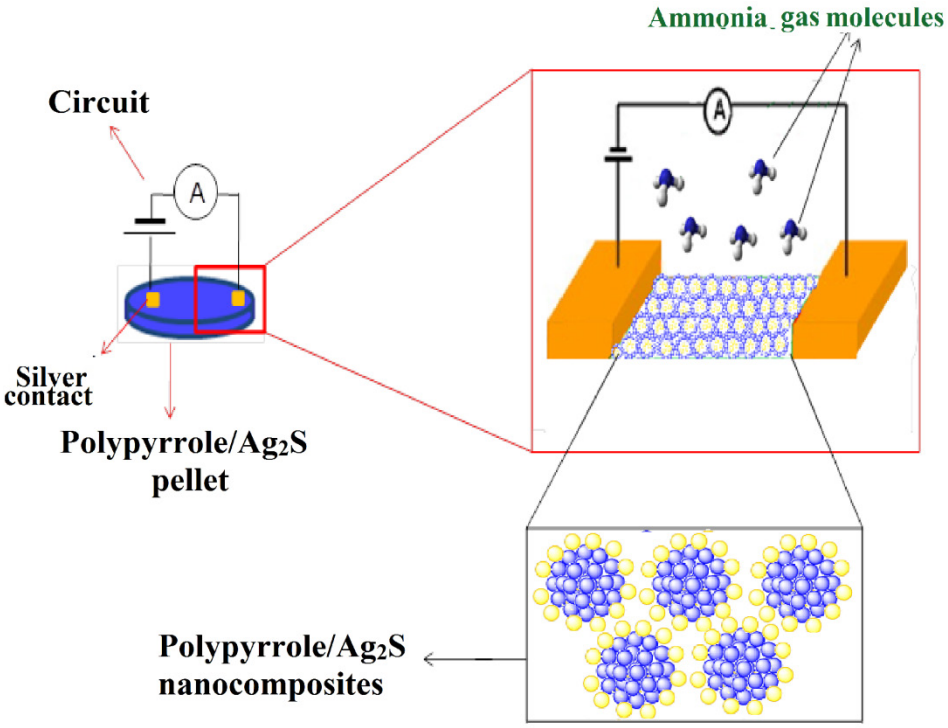

Figure 9. Pictorial representation of a two-probe gas sensing setup

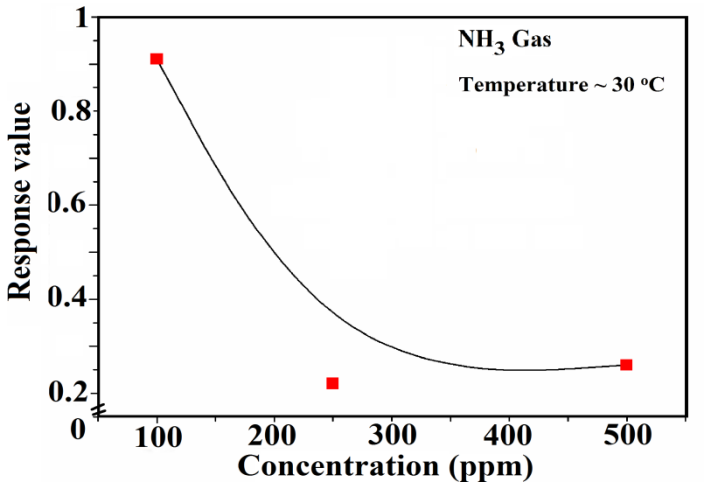

Figure 10. Response of PPy at different concentrations of NH_3 gas

Table 1. Response of PPy and PPy/Ag_2S NCs towards NH_3 gas

PPy and its nanocomposites	Response factor for different NH_3 concentrations		
	100 (ppm)	250 (ppm)	500 (ppm)
PPy	0.91 ± 0.09	0.22 ± 0.02	0.26 ± 0.03
PPy/1 wt% Ag_2S NPs (A1)	7.7 ± 0.70	0.69 ± 0.07	0.48 ± 0.05
PPy/2 wt% Ag_2S NPs (A2)	0.33 ± 0.03	0.43 ± 0.04	0.61 ± 0.06
PPy/3 wt% Ag_2S NPs (A3)	0.21 ± 0.02	0.32 ± 0.02	0.75 ± 0.07

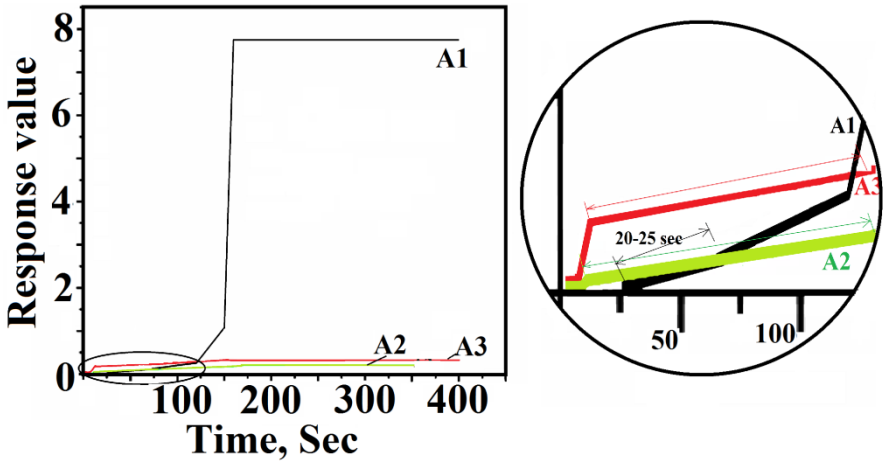

Figure 11. Response versus time graph of PPy/Ag_2S NCs for 100 ppm NH_3

Table 2. Comparison of sensor response of PPy/Ag_2S NCs with those of reported sensors

Nanocomposites Designation	Response factor for different NH_3 concentrations			Response Time (s)	Recovery time (s)	Reference
	100 (ppm)	250 (ppm)	500 (ppm)			
PPy/Ag_2S (1 wt%)	7.7	0.69	0.48	20	> 600	[Presesnt work]
PPy/Ag_2S (2 wt%)	0.33	0.43	0.61	150		
PPy/Ag_2S (3 wt%)	0.21	0.32	0.75	120		
PPy/ZnO	5	-	-	-	> 600	[6]
PPy/CdS (3 wt%)	0.74	4.2	0.33	20	-	[10]
PPy/WO_3@ 100 °C	25 (20 ppm)			25	120	[11]
PPy	1.18	-	-	90	>500	[27]
PPy nanowires	0.22 (290 ppm)			600	500	[35]
PPy nanowires	lower (200 ppm)			Higher		[36]
PPy	2.5	-	-	500	200	[37]
PPy-SnO_2	30	-	-	500	200	
PPy/Ag_2S (1 wt%)	0.65	0.97	1	20	> 600	[44]
PPy/Ag_2S (2 wt%)	0.33	0.38	0.5	20		
PPy/Ag_2S (3 wt%)	0.25	0.56	0.6	20		

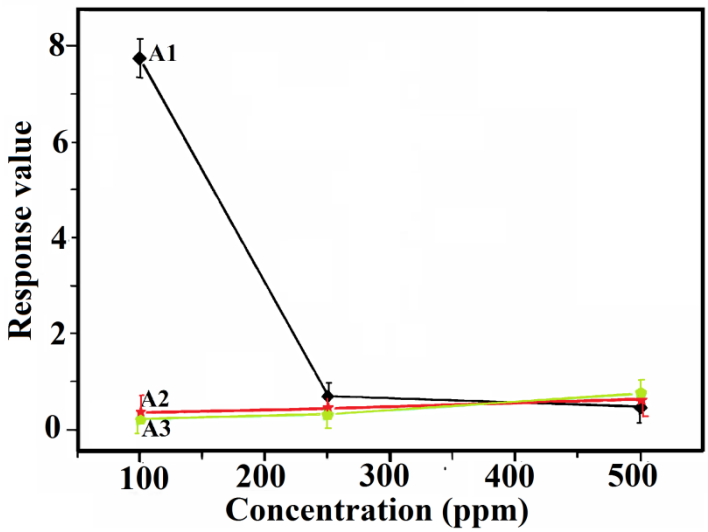

Figure 12. Response of PPy/Ag_2S NCs at different concentrations of NH_3 gas

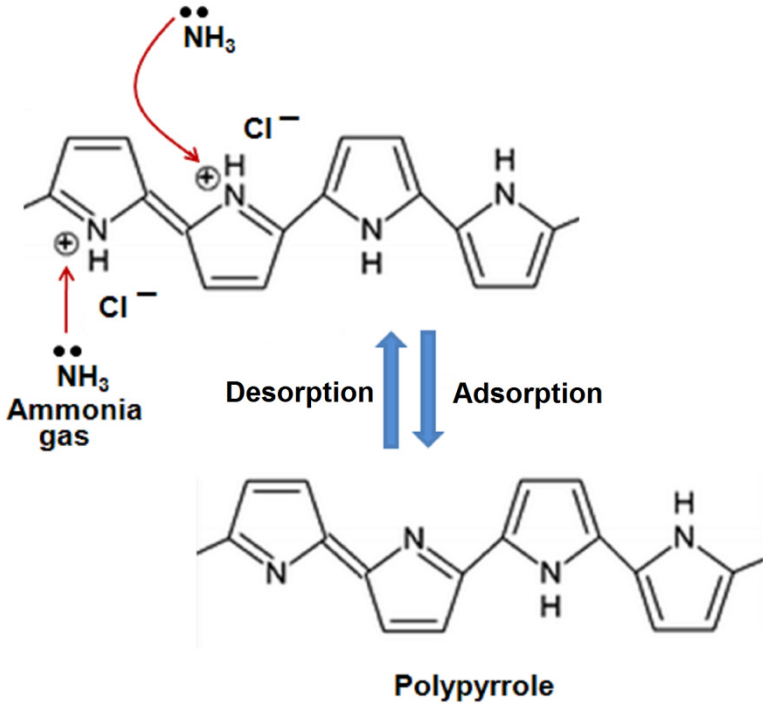

Scheme 2. Ammonia sensing mechanism by PPy sensor

NH_3 sensing was carried out in a two–probe gas sensing setup, as depicted in Figure 9. The change in resistance with time measured at a specified voltage gives the sensor response towards NH_3. Generally, an increase in resistance is observed for reducing gases such as NH_3. Figure 10 shows the response of pristine PPy when exposed to different concentrations of NH_3. Upon exposure to NH_3 gas, the PPy sensors registered a surge in their resistivity. The highest response factor of 0.91 was obtained for 100 ppm NH_3, while at subsequent higher concentrations the response factor decreased to 0.22 and 0.26 for 250 and 500 ppm, respectively. Such a low response to high concentrations of NH_3 resulted from the saturation of sensor surface with the gas molecules, which reduced its sensitivity. We performed three sensing cycles on a single sensor. Table 1 presents the results of gas responses of PPy and PPy/Ag_2S NCs with 10 % error. Our experiment shows that the sensor response is reproducible with an acceptable standard deviation of 0.026.

The PPy/Ag_2S (1 wt%) NC (A1) showed a remarkable increase in the sensor response (response factor ~ 7.7) towards 100 ppm NH_3 gas (Figure 11). However, a drop in the response factor was observed at higher Ag_2S NP content. Besides, the PPy/Ag_2S (1 wt%) NC (A1) also exhibited a very low response time of 20-25 s, while those of PPy/Ag_2S (2 and 3 wt%) NCs (A2 and A3) were reported to be over 100 s. The recovery times of all the samples were observed more than 10 min. The sensing performances of the PPy/Ag_2S (1, 2, and 3 wt%) NCs (A1, A2, and A3), in this research work, have been compared with that of the reported works, and the comparison is presented in Table 2. It is clear that the room temperature sensitivity of PPy/Ag_2S (1 wt%) NC (A1) is excellent as compared to those of the reported sensors. However, at higher gas concentrations, the surface saturation by ammonia gas resulted in a low value of response factor.

The change in the response factor of PPy/Ag_2S NC sensors with respect to changes in the NH_3 concentration is shown in Figure 12. It can be observed that an increase in the Ag_2S content led to a lowering of the sensor response; while PPy/Ag_2S (1 wt%) NC (A1) was highly responsive towards 100 ppm NH_3 gas, other compositions of PPy/Ag_2S NCs (A2 and A3) showed a lower response. As stated earlier, the n-type Ag_2S NPs result in charge localization in the p-type PPy and lowers the electrical conductivity of the NCs. Therefore, upon exposure to NH_3 gas, the reduction of PPy by NH_3 was restricted due to the already localized charges in the polymer. Hence, the NC sensors with a higher Ag_2S NP content showed a lower gas response.

The NH_3 sensing mechanism is illustrated in Scheme 2. When $FeCl_3$ doped PPy was exposed NH_3 gas to, an increment in current was observed. $FeCl_3$ doped PPy has cation radicals called polarons with Cl^- ions acting as counter ions to maintain the electro-neutrality of the polymer. Moreover, some amount of Fe^{2+} ions also exist within PPy. Therefore, PPy attains a partial oxidation state of up to +0.33 upon the adsorption of gas molecules. Thus, a higher oxidation state can be induced in PPy upon interaction with NH_3. Thus, PPy is a p-type semiconductor with holes being the main charge carriers in them. Upon exposure to NH_3, the gas molecules adsorbed on the sensor surface and the lone pair of electron in NH_3 gas is accepted by the holes in PPy. This results in a drop in the concentration of charge carriers in the PPy chains and consequently the conductivity decreases. Ammonia causes reduction or dedoping of doped PPy. When NH_3 gas molecules adsorb on the PPy surface, the lone pair of electron on the N atom is transferred to the PPy backbone, which has holes as charge carriers, leading to the formation of NH^+ moiety. The electron transfer between the NH_3 molecules and the PPy results in a reduction in the charge density of PPy, and thus an increase in its resistance is observed. Hence, following the adsorption of NH_3, the polymer becomes less conducting and the measured resistance increases. In the case of PPy/Ag_2S

NCs, an increase in the n-type Ag_2S NP content leads to charge localization in the p-type PPy, which drastically reduces the possibility of its accepting the electron pair from NH_3 when exposed to it [10,38-44]. Hence, the gas response of A2 and A3 NCs were much lower than that of A1 NC.

4. Conclusion

We studied the structural, morphological, and electrical properties and the sensing performances of PPy and PPy/Ag_2S NCs synthesized by ultrasound-assisted *in-situ* polymerization. Their morphological study revealed the formation of Ag_2S NPs, which were uniformly dispersed in the PPy matrix due to the effects of ultrasound. Moreover, spherical and porous PPy nanostructures were observed, which clustered in the presence of higher Ag_2S NP content. The current-voltage (I-V) characteristics implied a semiconducting nature for both PPy and its NCs. The electrical conductivity of the PPy/Ag_2S NC was found to be lower than that of pristine PPy when the Ag_2S NP content was 1 and 2 wt%; however, at 3 wt% Ag_2S NP content, the electrical conductivity registered a sharp increase as the NC attained the percolation threshold. PPy/Ag_2S NCs exhibited excellent sensitivity towards NH_3, which manifested as a drop in the sensor's conductivity. The underlying mechanism of NH_3 gas sensing is the reduction of PPy by the electron rich NH_3 gas molecules. The highest response factor of 7.7 was obtained by PPy/Ag_2S (1 wt%) for sensing of 100 ppm NH_3 concentration. However, increasing the gas concentration led to saturation of the sensor surface, which lowered the sensor response. Moreover, the sensor response of the PPy/Ag_2S NCs decreased as the Ag_2S NP content increased. This is because an increase in the n-type Ag_2S NP content led to charge localization in the p-type PPy, which drastically reduced the possibility of its accepting the electron pair from the NH_3 gas molecules when exposed to it. Overall, this work shows the potential of PPy/Ag_2S NCs for detection of NH_3 at room temperature through the synergistic effect of the PPy and the Ag_2S NPs.

Acknowledgments

Authors are thankful to University Grants Commission, New Delhi, Government of India for providing financial assistance under One Time Grant (UGC-BSR project no.: F.4-10/2010, dated 20 Sept., 2011) to carry out this research work. The authors Tanushree Sen and D.P. Hansora have contributed equally in writing this article.

References

[1] Said K., Ayesh A.I., Qamhieh N.N., Awwad F., Hisaindee S., *J. Alloy. Comp.,* 694, 1061, 2017.
[2] Markina M., Stozhko N., Krylov V., Vidrevich M., Brainina Kh., *Talanta,* 165, 563, 2017.
[3] Chaudhari P., Mishra S., *Measurement* 90, 468, 2016.
[4] Sen T., Shimpi N.G. and Mishra S. *Sens. Actuators B,* 190, 120, 2014.
[5] Janata J. and Josowicz M. *Nat. Mater.* 2, 24, 2003.
[6] Chougule M.A., Dalavi D.S., Mali S., Patil P.S., Moholkar A.V., Agawane G.L., Kim J.H., Sen S. and Patil V.B. *Measur.* 45, 1996, 2012.
[7] Geng L. and Wu S. *Mater. Res. Bull.* 48, 4343, 2013.
[8] Mishra S., Shimpi N.G. and Sen T. *J. Polym. Res.* 20, 49, 2013.
[9] Brezoi D.V. *J. Sci. Arts* 1, 53, 2010.
[10] Yeole B., Sen T., Hansora D.P. and Mishra S. *J. App. Polym. Sci.* 132(32), 42379, 2015.
[11] Ho T.A., Jun T.S. and Kim Y.S. *Sens. Actuators B* 185, 523, 2013.
[12] Nguyen L.Q., Phan P.Q., Duong H.N., Nguyen C.D. and Nguyen L.H. *Sens.* 13, 1754, 2013.
[13] Cui S., Pu H., Mattson E.C., Lu G., Mao S., Weinert M., Hirschmug C.J., Gajdardziska-Josifovska M. and Chen J. *Nanoscale* 4, 5894, 2012.
[14] Kuang Q. and Yang S. *Crys. Eng. Comm.* 16, 4940, 2014.
[15] Sharma S. and Madou M. *Philos. Trans. Res. Soc. A,* 370, 2448, 2012.
[16] Liu X., Cheng S., Liu H., Hu S., Zhang D. and Ning H. *Sens.* 12, 9665, 2012.
[17] Roy A.S., Koppalkar A.R. and Prasad M.V.N.A. *J. App. Polym. Sci.* 121(2), 675, 2011.
[18] Roy A.S., Koppalkar A.R. and Prasad M.V.N.A. *J. App. Polym. Sci.* 123(4), 1928, 2012.
[19] Roy A.S., Hegde S.G. and Parveen A. *Polym. Adv. Technol.* 25(1), 130, 2014.
[20] Parveen A., Koppalkar A.R. and Roy A.S. *IEEE Sens. J.* 12(9), 2817, 2012.
[21] Parveen A., Koppalkar A.R. and Roy A.S. *Sens. Letters,* 11(2), 242, 2013.
[22] Roy A.S., Koppalkar A.R. Sasikala, M. Machappa T. and Prasad M.V.N.A. *Sens. Letters* 9 (4), 1342, 2011.
[23] Adhikari B. and Majumdar S. *Prog. Polym. Sci.* 29, 766, 2004.
[24] Joshi A., Gangal S.A. and Gupta S.K. *Sens. Actuators B* 156, 938, 2011.
[25] Shimpi N.G., Mishra S., Hansora D.P. and Savdekar U. Indian Patent 3179/MUM/2013, 2013.
[26] Hansora D.P., Shimpi N.G. and Mishra S. *JOM* 67(12), 2855, 2015.
[27] Shimpi N.G., Mali A.D., Hansora D.P. and Mishra S. *Nanosci. Nanoeng.* 3, 8, (2015)
[28] Wu T.M., Chang H.L. and Lin Y.W. *Polym. Int.* 58, 1065, 2009.
[29] Lu Y., Shi G., Li C. and Liang Y. *J. App. Polym. Sci.* 70, 2169, 1998.
[30] Li X.G., Li A., Huang M.R., Liao Y. and Lu Y.G. *J. Phys. Chem. C* 114, 19244, 2010.
[31] Hamilton A. and Breslinm C.B. *Electrochim Acta* 145, 19, 2014.
[32] Nalage S.R., Navale S.T. and Patil V.B. *Measurement* 46, 3268, 2013.
[33] Montoya P., Mejía S., Gonçales V.R., Torresi S.I.C. de and Calderón J.A. *Sens. Actuators B: Chem.,* 213, 444, 2015.
[34] Yang X., Li L. and Yan F. *Sens. Actuators B: Chem.,* 145, 495, 2010.
[35] Chih Y.K. and Yang M.C. *J. Taiwan Inst. Chem. Eng.* 45, 833, 2014.
[36] Yang X., Li L. and Zhao Y. *Synt. Met.* 160(17), 1822, 2010.
[37] Liu F., Yuan Y., Li L., Shang S., Yu X., Zhang Q., Jiang S. and Wu Y. *Comp. Part B: Eng.* 69, 232, 2015.
[38] Ullah H., Ayubb K. Ullah Z., Hanif M., Nawaz R., Shah A.H.A, Bilal S, *Synt. Met.* 172, 14-20 (2013).
[39] Scott D., Cooney M.J. and Liaw B.Y., *J. Mater. Chem.,* 18, 3216-3222, 2008.
[40] Dunst K.J., Cysewska K., Kalinowski P., Jasiński P., IMAPS Poland, Conference, IOP Conf. Series: *Mater. Sci. Eng.* 104, 012028, 2015.
[41] Hernandez S.C., Chaudhuri D., Chen W., Myung N.V., Mulchandani A., *Electroanal.* 19, (19-20), 2125, 2007.
[42] Garg R., Kumar V., Kumar D., and Chakarvarti S.K., *J. Sens. Instrument.* 3(1) 1, 2015.
[43] Bagchi S., and Ghanshyam C. *J. Phys. D: Appl. Phys.* 50, 105302, 10, 2017.
[44] Yeole B., Sen T., Hansora D.P. and Mishra S. *Mater. Res.* 19(5), 999, 2016.